



Cite this: *Phys. Chem. Chem. Phys.*,
2020, 22, 1313

Thermally activated delayed fluorescence emitters with dual conformations for white organic light-emitting diodes: mechanism and molecular design†

Feiyan Li, Guanyu Jiang, Muzhen Li, Jianzhong Fan,  Yuzhi Song,
Chuan-Kui Wang* and Lili Lin  *

Thermally activated delayed fluorescence (TADF) molecules with dual emission have great potential for use as single emitters in white organic light-emitting diodes (WOLEDs). In this paper, the light-emitting mechanisms of PTZ-TTR and PTZ-Ph-TTR with blue-orange dual emission are studied systematically. The near-planar and near-orthogonal conformations are responsible for the blue and orange emission, respectively. For PTZ-TTR, the near-orthogonal conformation is only generated by the transformation from the near-planar conformation, while the near-orthogonal conformation of PTZ-Ph-TTR can be generated by both excitation and transformation. This results in relatively strong orange emission in PTZ-Ph-TTR. In addition, the TADF mechanism is investigated, and two up-conversion pathways are revealed for both molecules. Based on the comparison of the photophysical properties of PTZ-TTR in toluene and the aggregation state, we find that aggregation could induce a smaller energy gap between the first singlet excited state and the first triplet excited state. Besides, the substitution effect of donors on light-emitting properties is studied, and the design rules for emitters with dual conformations and compensatory emission are proposed. Our theoretical results would favor the understanding of the light-emitting mechanism as well as the design of new-type TADF emitters for WOLEDs.

Received 11th October 2019,
Accepted 29th November 2019

DOI: 10.1039/c9cp05552e

rsc.li/pccp

1 Introduction

Recently, white organic light-emitting diodes (WOLEDs) have received widespread attention and achieved significant development due to their potential application in solid-state lighting devices.^{1–3} Nevertheless, WOLEDs are usually composed of two or more components where two complementary colors (orange and blue) or three primary colors (red, green and blue) simultaneously illuminate to form white light. Thus sophisticated device structures are needed for WOLEDs to finely and accurately optimize the energy transfer process and exciton distribution, which also leads to increased cost and repetition reduction directly.^{2,4–9} One way to solve this problem is to develop a single emitter that can display white emission, and most of them are realized by using polymers with multiple chromophores, monomers and excimer emission, excited-state intramolecular proton transfer (ESIPT),

vibration-induced emission (VIE) plus aggregation-induced emission (AIE) or hybrid fluorescence/phosphorescence systems.^{10–18} Recently, Zhang's group proposed a novel concept to develop thermally activated delayed fluorescence (TADF) fluorophores with dual conformations as single emitters for highly efficient WOLEDs.¹⁴ TADF emitters which can realize full exciton usage efficiency have attracted great attention recently, and also achieved significant progress.^{19,20} Most of the TADF emitters are composed of electron-donating (donors, D) groups and electron-attractive (acceptor, A) groups based on the steric effect, which can favor the separation of electron distribution in the transition orbitals.^{21,22} Although several TADF emitters have been found to have multiple or dual conformations, a few were reported as emitters for WOLEDs.²³ Theoretical studies on TADF emitters with dual conformations used in WOLEDs could help one better understand the relationship between conformations and photophysical properties.

In this work, we focus on two molecules: 2-(10*H*-phenothiazin-10-yl)thianthrene 5,5,10,10-tetraoxide (PTZ-TTR) and 2-(4-(10*H*-phenothiazin-10-yl)phenyl)thianthrene 5,5,10,10-tetraoxide (PTZ-Ph-TTR) (see Fig. 1(a)) recently reported by Zhang's group.¹⁴ The light-emitting properties of the two molecules in toluene are studied based on first-principles calculations to figure out the influence of connection groups. In addition, the photophysical

Shandong Key Laboratory of Medical Physics and Image Processing & Shandong Provincial Engineering and Technical Center of Light Manipulations, School of Physics and Electronics, Shandong Normal University, Jinan 250358, China.
E-mail: ckwang@sdu.edu.cn, linll@sdu.edu.cn

† Electronic supplementary information (ESI) available: Energy levels, RMSD, NTOs of PTZ-TTR in the solid phase; geometries of all systems designed; charge differences of donors in S₁ and S₀, and NTOs for all systems. See DOI: 10.1039/c9cp05552e

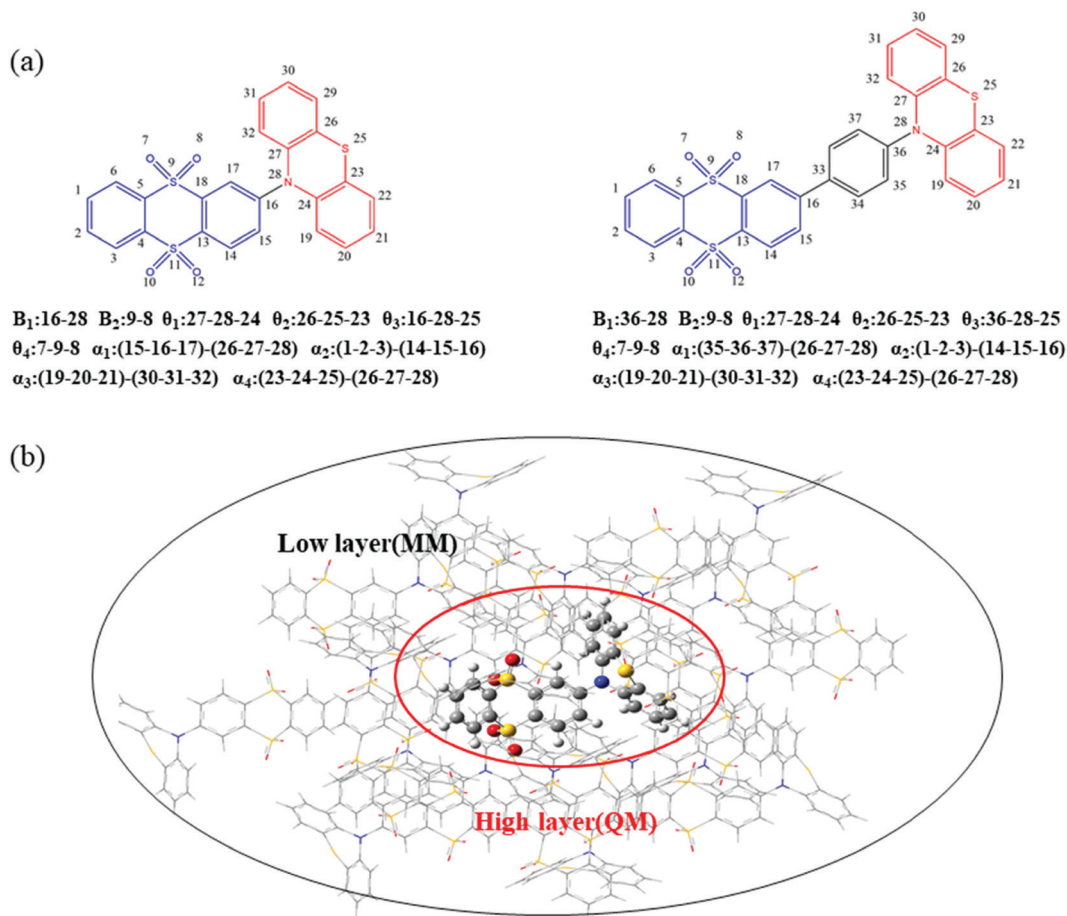


Fig. 1 (a) Chemical structures of PTZ-TTR (left) and PTZ-Ph-TTR (right) with atomic labels, interesting bond lengths, bond angles, and dihedral angles. (b) ONIOM model: the central PTZ-TTR molecule is treated as the high layer and surrounding molecules are regarded as the low layer.

properties of PTZ-TTR are also studied, and its environmental effects could be revealed. Finally, several molecules designed based on TTR with different donor groups are theoretically studied, which could favor the design of TADF molecules used as WOLEDs.

2 Theoretical methods and calculation details

In this work, the molecules in the ground state (S_0) are optimized using the density functional theory (DFT) method,

and the time-dependent density functional theory (TD-DFT) method is used to optimize the excited states of molecules (such as the first excited singlet state (S_1) and the first triplet excited states (T_1)). Frequency calculations were performed to confirm the stability of S_0 , S_1 , and T_1 . Since both molecules are composed of D and A units, their excited states are quite dependent on the functionals. Consequently, several functionals with different percentages of Hartree–Fock exchange (HF%), including B3LYP, PBE0, PBE33, BMK, and M06-2X, are tested and the PBE0 functional is found more suitable based on the calculation of emission wavelengths (as shown in Table 1).

Table 1 Emission wavelengths calculated using different functionals for PTZ-TTR and PTZ-Ph-TTR in toluene and in the aggregate state

	HF%	Toluene				Aggregation
		PTZ-TTR-p	PTZ-TTR-o	PTZ-Ph-TTR-p	PTZ-Ph-TTR-o	PTZ-TTR-p
Exp. ^a	—	435	635	450	600	440
B3LYP	20	—	698	462	661	—
PBE0	25	391*	643	435	603	405
PBE33	33	—	557	392	513	—
BMK	42	—	494	372	451	—
M062X	54	—	452	356	405	—

^a Exp. represents experimental data.

Consequently, the PBE0 functional and the 6-31G(d) basis set are adopted in our calculations. The polarizable continuum model (PCM) is used to simulate the solvent effect,²⁴ and the combined quantum mechanics and molecular mechanics (QM/MM) approach is used to consider the surrounding effect in the solid phase.^{25–28} The QM/MM calculation is realized in the ONIOM model, which is proven to be reliable in our previous study.^{22,28–30} The initial configuration of PTZ-TTR in the solid phase is built based on the crystal structure detected experimentally.¹⁴ In our calculation, the two-layer ONIOM model is adopted (as seen in Fig. 1(b)), where the central molecule is treated as a high layer and calculated using the QM method, and the surrounding molecules are considered to be a low layer and are computed using the MM method. For the MM calculation, the universal force field (UFF) is used, which has also been proven reliable.³¹ In addition, the electronic embedding scheme is adopted in the ONIOM calculation. All the above calculations are performed using the Gaussian 16 software package.³²

For the fluorescence radiative decay rate of TADF molecules, we can calculate it using Einstein's spontaneous emission formula:

$$k_r = \frac{f \Delta E_{fi}^2}{1.499} \quad (1)$$

where f is the oscillator strength and ΔE_{fi} is the vertical emission energy with the unit of wavenumbers (cm^{-1}).³³

What's more, the intersystem crossing (ISC) rate constant between two electronic states with different spin multiplicities can be written as:

$$k_{ISC} = \frac{1}{\hbar} \langle \Phi_f | \hat{H}^{SO} | \Phi_i \rangle \int_{-\infty}^{\infty} dt [e^{i\omega_{if}t} Z_i^{-1} \rho_{ISC}(t, T)] \quad (2)$$

where Z_i is the partition function and $\rho_{IC}(t, T)$ is the thermal-vibration correlation function. The reverse intersystem crossing (RISC) rate can also be calculated using eqn (2). The ISC and RISC rates in toluene and the solid phase are all calculated using MOMAP (Molecular Materials Property Prediction Package).³⁴

For further information about the methodology and application of this formalism, one could refer to ref. 35–37.

3 Results and discussions

3.1 Geometric structures and electronic structures

Since the excited states of the molecules studied here are functional dependent, the functionals are tested based on the calculation of emission wavelengths (as shown in Table 1). Two conformations of both PTZ-TTR and PTZ-Ph-TTR in S_1 are found with different functionals. For convenience, the conformation with PTZ which is approximately parallel to TTR is labeled with - p, and the conformation with the almost orthogonal angle between TTR and PTZ is labeled with - o. It is found that the calculated emission wavelengths for PTZ-Ph-TTR-p and PTZ-Ph-TTR-o in toluene are 435 nm and 603 nm respectively, in agreement with the experimental results (450 nm and 600 nm). The emission wavelengths of PTZ-TTR-p and PTZ-TTR-o (391 nm and 643 nm) in toluene are also in good agreement with the experimental values (435 nm and 635 nm). One should notice that the S_1 geometry of PTZ-TTR-p could be not obtained by optimization with any functional. The emission wavelength for PTZ-TTR-p in toluene is calculated based on the geometry without virtual frequency. However, the geometry of PTZ-TTR-p in S_1 can be obtained by optimization in the solid phase, and the emission wavelength (405 nm) calculated also agrees well with the experimental counterpart (440 nm). Consequently, the PBE0 functional is adopted in all the QM calculations.

Some important geometric parameters of optimized S_0 , S_1 , and T_1 for PTZ-TTR and PTZ-Ph-TTR in toluene with PBE0 are listed in Tables 2 and 3 respectively. It is found that the main difference between PTZ-TTR-p and PTZ-TTR-o is the dihedral angle between D and A (α_1). The α_1 for PTZ-TTR in S_0 is about 11° and 87° respectively. Simultaneously, the main difference between PTZ-Ph-TTR-p and PTZ-Ph-TTR-o in S_0 is also found to be the dihedral angle in α_1 (12° and 89°). When the molecule is excited to S_1 , there are significant changes in the bond angles (θ_3) and dihedral angles (α_1 – α_4). The changes between S_0 and S_1

Table 2 Geometry parameters of the S_0 , S_1 , and T_1 states of PTZ-TTR in toluene^a

Geometry	Toluene									
	PTZ-TTR-p					PTZ-TTR-o				
	S_0	S_1	T_1	$ \Delta s_{0-S_1} $	$ \Delta s_{1-T_1} $	S_0	S_1	T_1	$ \Delta s_{0-S_1} $	$ \Delta s_{1-T_1} $
B_1	1.388	1.422	1.390	0.034	0.032	1.423	1.447	1.446	0.024	0.001
B_2	1.463	1.474	1.469	0.011	0.005	1.462	1.473	1.473	0.011	0
θ_1	114.780	115.219	115.139	0.439	0.08	120.908	124.780	124.775	3.872	0.005
θ_2	97.729	98.828	97.609	1.099	1.219	98.963	103.092	103.089	4.129	0.003
θ_3	123.223	136.314	137.219	13.091	0.905	162.284	179.696	179.011	17.412	0.685
θ_4	119.312	117.742	117.932	1.57	0.19	119.723	117.194	117.221	2.529	0.027
α_1	10.754	7.470	7.524	3.284	0.054	87.070	89.067	88.543	1.997	0.524
α_2	135.120	119.219	125.622	15.901	6.403	133.894	123.505	123.626	10.389	0.121
α_3	131.619	143.172	136.207	11.5534	6.965	148.054	178.703	178.229	30.649	0.474
α_4	133.300	140.748	135.103	7.448	5.645	135.182	178.190	177.532	43.008	0.658

^a B , θ , and α (marked in Fig. 1(a)) represent the bond length, bond angle, and dihedral angle, respectively. Δ represents the variation between the two states.

Table 3 Geometry parameters of S_0 , S_1 , and T_1 states of PTZ-Ph-TTR in toluene^a

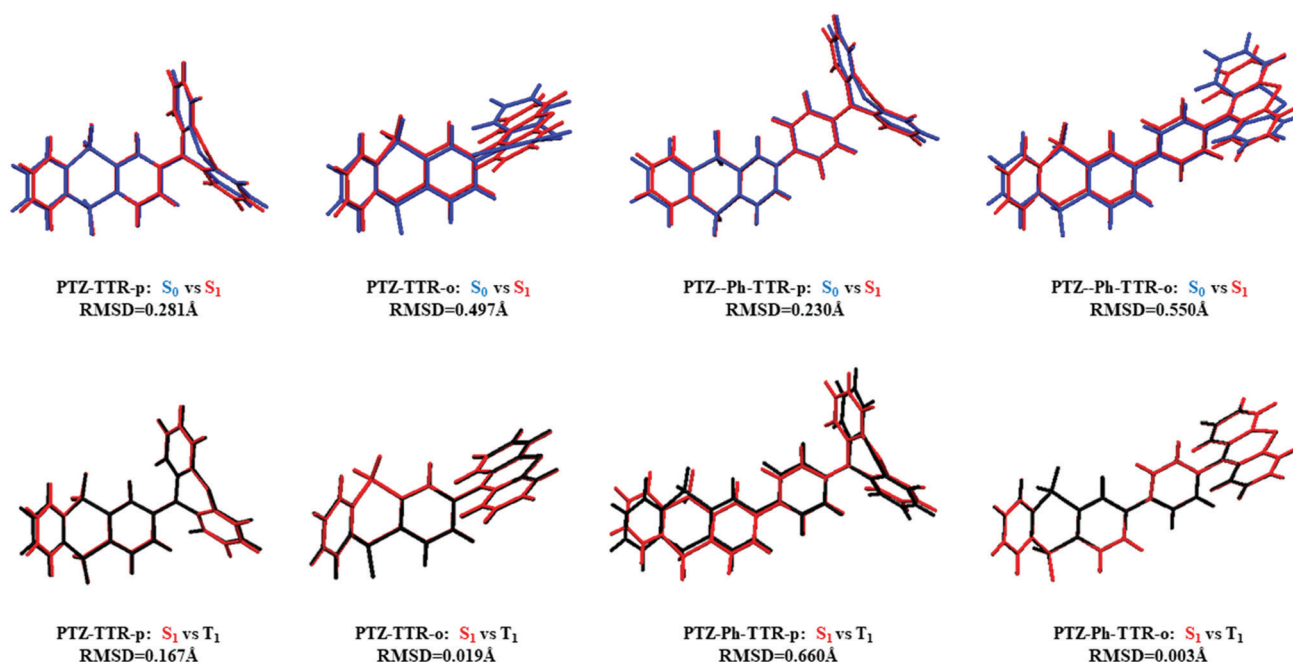
Geometry	Toluene									
	PTZ-Ph-TTR-p					PTZ-Ph-TTR-o				
	S_0	S_1	T_1	$ \Delta_{S_0-S_1} $	$ \Delta_{S_1-T_1} $	S_0	S_1	T_1	$ \Delta_{S_0-S_1} $	$ \Delta_{S_1-T_1} $
B_1	1.399	1.396	1.383	0.003	0.013	1.428	1.447	1.446	0.019	0.001
B_2	1.463	1.474	1.467	0.011	0.018	1.462	1.471	1.471	0.009	0
θ_1	114.775	115.364	114.576	0.589	0.788	121.055	124.785	124.770	3.73	0.015
θ_2	97.664	98.014	97.353	0.35	0.661	99.012	103.050	103.048	4.038	0.002
θ_3	123.725	135.309	131.769	11.584	3.54	163.732	179.760	179.716	16.028	0.044
θ_4	119.433	116.961	118.433	2.472	1.472	119.573	117.559	117.575	2.014	0.016
α_1	11.821	4.757	3.399	7.064	1.358	89.280	89.842	89.664	0.562	0.178
α_2	133.913	120.666	127.791	13.247	7.125	134.140	127.093	127.162	7.047	0.069
α_3	132.823	139.129	133.385	6.306	5.744	147.123	179.649	179.619	32.526	0.030
α_4	132.931	138.136	133.307	5.205	4.829	135.748	179.522	179.499	43.774	0.023

^a B , θ , and α (marked in Fig. 1(a)) represent the bond length, bond angle, and dihedral angle, respectively. Δ represents the variation between the two states.

of the five angles of PTZ-TTR-p are about 12° , 3° , 16° , 12° , and 7° ; meanwhile, those of PTZ-TTR-o are about 16° , 2° , 10° , 31° , and 43° respectively. It is found that the change of α_1 and α_2 in PTZ-TTR-o is smaller than that in PTZ-TTR-p. However, more significant variation is found for θ_3 , α_3 , and α_4 in PTZ-TTR-o. Specifically, the planarity of the acceptor (α_2) becomes worse in both near-planar and near-orthogonal conformations, while the donor tends to form a plane especially for the near-orthogonal conformation. By comparing S_1 and T_1 , we can see that the main changes for PTZ-TTR-p are α_2 (6°), α_3 (7°), and α_4 (6°), while little difference is found for PTZ-TTR-o. Similar situations can also be found in PTZ-Ph-TTR. It is found that the bond lengths and most bond angles of PTZ-Ph-TTR only undergo a slight change upon excitation, whereas bond angles (θ_3) and dihedral angles (α_1 – α_4) change obviously, and the trend of change is the same as that of PTZ-TTR when it is excited from

S_0 to S_1 . By comparing the difference between S_1 and T_1 , we can find the variation of bond angles and dihedral angles for PTZ-Ph-TTR-p, while no significant change is involved for PTZ-Ph-TTR-o. Comparing PTZ-TTR with PTZ-Ph-TTR, we find that the phenyl unit inserted between D and A could influence the geometric variation to some extent, while the variation tendency is similar for both systems.

At the same time, the root mean square displacement (RMSD) is calculated to quantitatively characterize the geometric changes in excitation (as shown in Fig. 2).³⁸ When the molecule is excited from S_0 to S_1 , smaller RMSD values are found for the near-planar conformations (0.281 Å and 0.230 Å) than the near-orthogonal conformations (0.497 Å and 0.550 Å). Nevertheless, comparing the RMSD values between S_1 and T_1 , a larger variation is found for the near-planar conformations (0.167 Å and 0.660 Å) than the near-orthogonal conformations (0.019 Å and 0.003 Å). This further

**Fig. 2** Geometric deviation and RMSD values for PTZ-TTR and PTZ-Ph-TTR between S_0 (blue), S_1 (red) and T_1 (black) in toluene.

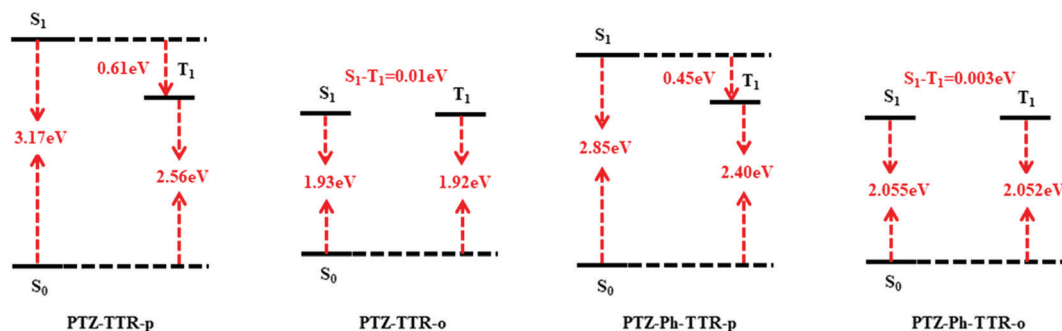


Fig. 3 Energy levels for PTZ-TTR and PTZ-Ph-TTR in toluene respectively. The energy of S_0 for PTZ-TTR-o is 0.17 eV higher than that for PTZ-TTR-p. The energy of S_0 for PTZ-Ph-TTR-o is 0.03 eV higher than that for PTZ-Ph-TTR-p.

confirms the conclusion that the variation tendency for two molecules is similar. Of course, one can notice that the RMSD value for S_1 - T_1 of PTZ-Ph-TTR-p is much larger than other values. This should come from the variation of the dihedral angle change between PTZ or TTR and the phenyl unit. All the geometries of both ground states and excited states are obtained using the PBE0 functional in QM calculations.

For TADF molecules, the energy gap between S_1 and T_1 plays a principal role in the RISC process, so the energy levels of all conformers in toluene are calculated with PBE0 as illustrated in Fig. 3. It is found that there is only one triplet state which is lower in energy than S_1 . The energy gaps between S_1 and T_1 for PTZ-TTR-o and PTZ-Ph-TTR-o are 0.01 eV and 0.003 eV, respectively, while they become 0.61 eV and 0.45 eV for PTZ-TTR-p and PTZ-Ph-TTR-p, respectively. This indicates that the energy gap between S_1 and T_1 can be effectively reduced by inserting the phenyl unit between D and A. Since TADF is generally realized by up-conversion from T_1 to S_1 , the small energy gap between S_1 and T_1 should be the basic condition for the up-conversion. Based on the calculation results above, we deduce that the near-orthogonal configurations are responsible for the realization of up-conversion. Of course, the other mechanism may also exist such as the up-conversion from T_2 to S_1 during excited-state intramolecular proton transfer (ESIPT).³⁹

We are also wondering how two conformations are transformed and whether there are other pathways for up-conversion. The potential energy curves of PTZ-TTR and PTZ-Ph-TTR in toluene are plotted as shown in Fig. 4. It is found that there are two stable conformations for both PTZ-TTR and PTZ-Ph-TTR in the ground state, and the near-planar conformation is lower in energy than the near-orthogonal conformation. The energy barrier from PTZ-TTR-p to PTZ-TTR-o is about 0.22 eV, while the barrier backward is only about 0.05 eV. This indicates that PTZ-TTR-o is rarely available since it can transform into the near-planar conformation easily. From the potential energy curve of S_1 , we find that the PTZ-TTR-p conformation is not a stable configuration, because there is almost no barrier for it going to the near-orthogonal conformation. This is in agreement with our former calculation results that the S_1 geometry of PTZ-TTR-p cannot be obtained in toluene. In addition, we find that the energy barrier from PTZ-TTR-o to PTZ-TTR-p is as high as 0.98 eV, which makes the backward transformation difficult. This also means that the geometry of PTZ-TTR-o in S_1 is more stable than the near-planar conformation. The potential energy curve of T_1 is also plotted, and both the near-planar and the near-orthogonal conformations are available. However, the energy barrier from PTZ-TTR-p to PTZ-TTR-o is almost barrierless (0.006 eV), which also indicates that the transformation from PTZ-TTR-p to PTZ-TTR-o is quite fast. Similar to the

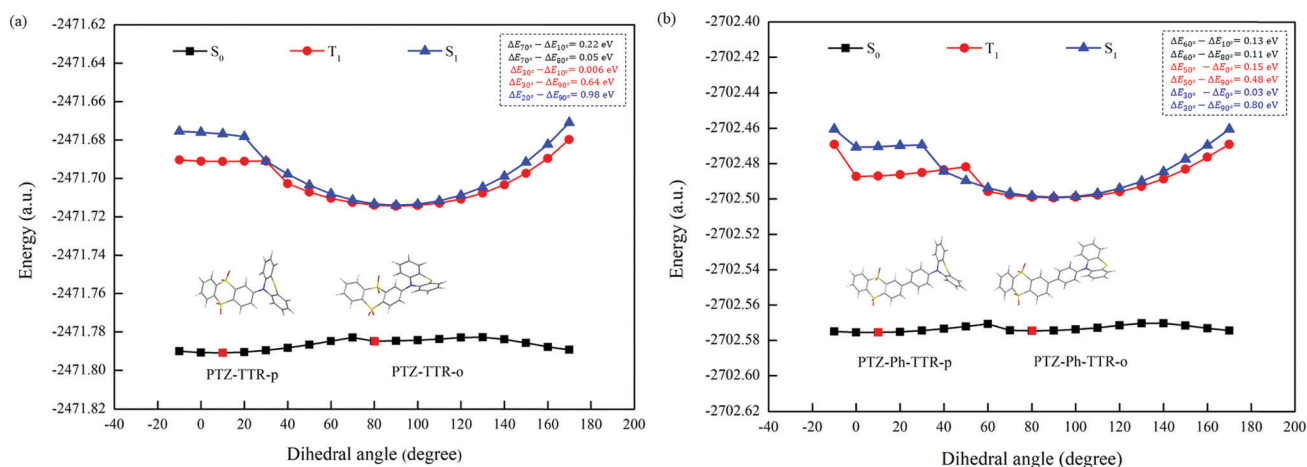


Fig. 4 Potential energy curves of S_0 (black), S_1 (blue) and T_1 (red) for PTZ-TTR (a) and PTZ-Ph-TTR (b) in toluene.

potential energy curve of S_1 , the backward transformation is more difficult (with an energy barrier of 0.64 eV). It is also obvious that the energy gap between S_1 and T_1 in PTZ-TTR-o is quite small, which means that the up-conversion from T_1 to S_1 should be possible. One should also notice that there is also one cross point between the potential energy curves of S_1 and T_1 , and thus we deduce that it is also possible that the conversion from T_1 to S_1 may also happen during the conformation transformation process. The discontinuities in the energy surface of T_1 and S_1 at 30° (in Fig. 4(a)) and 50° (in Fig. 4(b)) should be induced by the coupling between two states. In these conformations, the singlet state and the triplet state will mix, and thus result in a significant change of energy. The same as that in PTZ-TTR, there are also two stable conformations in the ground state for PTZ-Ph-TTR. The energy barrier from PTZ-Ph-TTR-p to PTZ-Ph-TTR-o is 0.13 eV and the backward energy barrier is 0.11 eV. This indicates that both conformations may exist. Different from PTZ-TTR, the configuration of PTZ-Ph-TTR-p in S_1 can be obtained by optimization. Two local minima are found for PTZ-Ph-TTR. The energy barrier from PTZ-Ph-TTR-p to PTZ-Ph-TTR-o is about 0.03 eV and the backward barrier is 0.80 eV, which means that it is easy for PTZ-Ph-TTR-p to transform to PTZ-Ph-TTR-o. A similar energy curve can be found for T_1 , while the energy barrier from PTZ-Ph-TTR-p to PTZ-Ph-TTR-o is a little larger (0.15 eV). This indicates that the transformation for

PTZ-Ph-TTR in T_1 is a little difficult. Nevertheless, we can see that there is also one cross point between the energy curves of T_1 and S_1 , which may provide the way for up-conversion from T_1 to S_1 .

Based on the analysis of the calculated potential energy curve of two systems with PBE0, we deduce that there is only one conformation for PTZ-TTR in the ground state, while both near-planar and near-orthogonal conformations may exist for PTZ-Ph-TTR. When the molecule is excited, only the near-planar conformation in S_1 (or T_1) can be obtained directly for PTZ-TTR. The near-orthogonal conformation in S_1 (or T_1) for PTZ-TTR is generated only by the transformation of PTZ-TTR-p. However, both near-planar and near-orthogonal conformations in S_1 (or T_1) can be obtained for PTZ-Ph-TTR, and there are two pathways to generate S_1 or (T_1) of PTZ-Ph-TTR-o. This could explain why the emission at 600 nm for PTZ-Ph-TTR is relatively stronger than the emission at 635 nm for PTZ-TTR.

In order to gain a deeper understanding of the photophysical properties of the molecules in toluene, the natural transition orbitals (NTOs) calculated with PBE0 are analyzed (as shown in Fig. 5). Since more than one pair of molecular orbitals contribute to the transition, it is more convenient to use NTOs to analyze the transition properties. NTO refers to finding a compact orbital representation for the electronic transition density matrix, and it can simplify the transition problem that can be described by multiple orbital transition modes.⁴⁰ Consequently, it has become

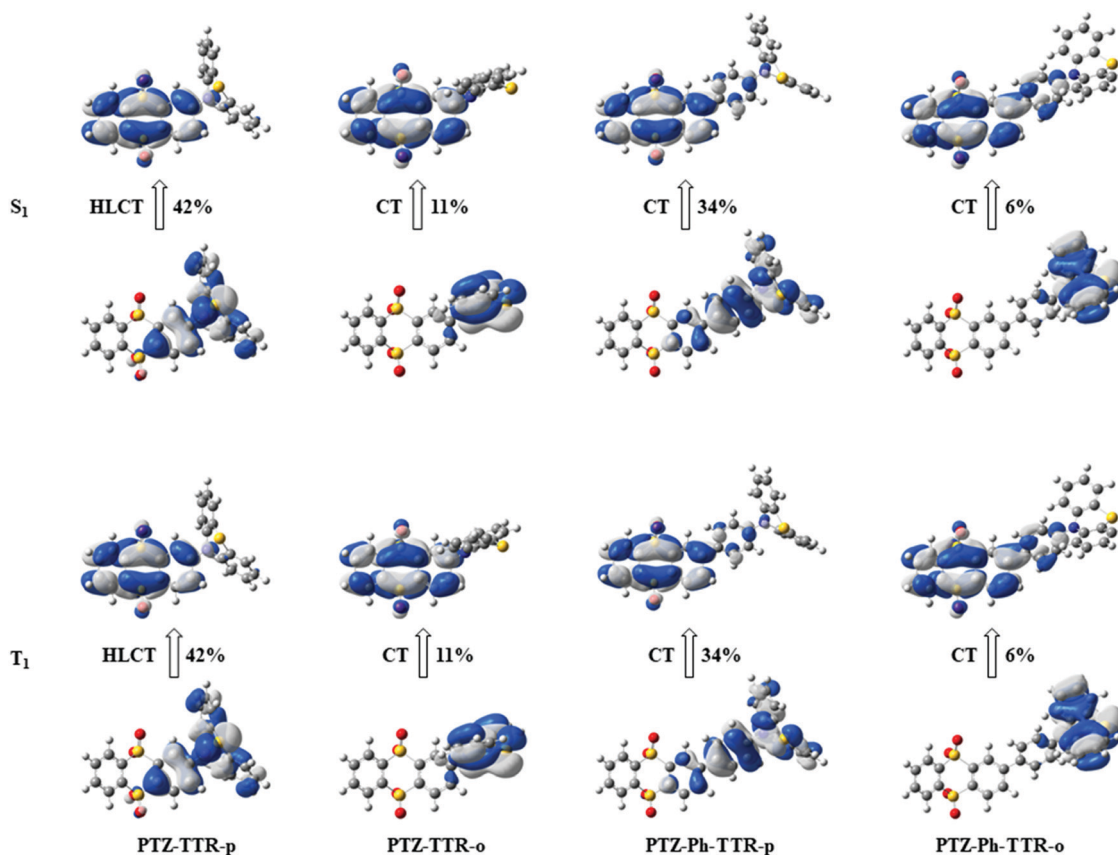


Fig. 5 Natural transition orbitals for S_1 (up) and T_1 (below) for PTZ-TTR and PTZ-Ph-TTR in toluene, respectively. The values in the right side of the arrow are the LE proportion upon excitation.

a very popular and useful way to analyze electron excitation obtained by single-reference methods. It is found that the transition from the hole to the particle predominates in both S_1 and T_1 . The local-excited (LE) state (with the particle-hole overlap in 75–100%) is a highly efficient radiation state, which produces a large transition moment and a large orbital overlap. The charge-transfer (CT) state (with the overlap in 0–40%) is depicted as a pair of coulomb-bound holes and electrons that reside on the donor and acceptor, respectively, and the electron transition due to the complete separation of the orbitals results in a smaller ΔE_{ST} energy gap.^{41,42} The hybrid local-excited and charge transfer (HLCT) state (with the overlap in 40–75%) is where LE and CT are highly mixed (or hybridized).^{42,43} The transition property is analyzed based on the overlap between the hole and particle wave function which is seen as the LE component. The overlap integral can be expressed as follows:

$$S_r = \int \sqrt{\rho^{\text{hole}}(r)\rho^{\text{ele}}(r)}dr = \int \sqrt{|\phi_i(r)|^2|\phi_j(r)|^2}dr = \int |\phi_i(r)||\phi_j(r)|dr$$

We can see that the S_1 state of PTZ-TTR-p is the HLCT state with an overlap in 42%, while PTZ-Ph-TTR-p in S_1 becomes a clear CT state (with LE component 34%). What's more, the S_1 and T_1 states for both PTZ-TTR-o and PTZ-Ph-TTR-o are typical CT states, which could result in a small energy gap between S_1 and T_1 . In addition, the LE component is reduced when a phenyl unit is inserted between D and A, which means a smaller energy gap will be obtained for PTZ-Ph-TTR-o. This is also in agreement with our calculated results (0.01 eV and 0.003 eV for PTZ-TTR-o and PTZ-Ph-TTR-o, 0.61 eV and 0.45 eV for PTZ-TTR-p and PTZ-Ph-TTR-p).

3.2 Decay rates of excited states

Based on the energy levels of excited states, we find that there is only one triplet state (T_1) which is lower in energy than the S_1 state, and the energy gap between S_1 and T_1 is quite small for the near-orthogonal conformations. The up-conversion from T_1 to S_1 should be quite possible in both PTZ-TTR-o and PTZ-Ph-TTR-o. Of course, the spin-orbit coupling (SOC) is also an important parameter that influences the up-conversion process. The SOC constants between S_1 and T_1 in toluene are calculated using the Dalton package,⁴⁴ and the corresponding data are organized in Table 4. The results show that the SOC constants between S_1 and T_1 in the near-planar conformations are larger than those in the near-orthogonal conformations,

which is more conducive to the collection of triplet excitons. The SOC values are also related to the transition properties of S_1 and T_1 . Since both S_1 and T_1 of the near-planar conformations have more LE component than the near-orthogonal conformations, larger SOC values are expected.^{23,45} In addition, both the ISC and RISC rates are calculated. It is found that the ISC rate of PTZ-TTR-p ($2.20 \times 10^7 \text{ s}^{-1}$) is larger than that of PTZ-TTR-o ($2.78 \times 10^6 \text{ s}^{-1}$). A larger ISC rate can also be found for PTZ-Ph-TTR-p than that for PTZ-Ph-TTR-o. Although the energy gap between S_1 and T_1 for the near-orthogonal conformations are smaller than that for the near-planar conformations, smaller ISC rates are found for the former due to smaller SOC constants. However, the RISC rates calculated for the near-orthogonal conformations are much larger than those of the near-planar conformations, since the energy gap plays a more significant role in the up-conversion process than the SOC constants. Consequently, the up-conversion can only happen in the near-orthogonal systems. This also means that the near-orthogonal conformations are responsible for the exciton collection.

Besides, the radiative rates of S_1 are also calculated. The radiative decay rates (k_r) of the near-planar conformations are about three orders of magnitude higher than those of the near-orthogonal conformations, because a larger oscillator strength is found for the near-planar conformations. One can notice that the radiative rate for PTZ-Ph-TTR-o is 0, due to the fact that the calculated oscillator strength of the S_1 state is zero. This is also the reason that the calculated fluorescence efficiency is zero. Actually, the oscillator strength of PTZ-TTR-o is also quite small (0.0001), quite close to zero. With such a small oscillator strength, the radiative rate calculated for PTZ-TTR-o is $1.61 \times 10^4 \text{ s}^{-1}$. This seems to disagree with the experimental results that the emissions from near-orthogonal conformations are found. To further explore the reason why the emission of near-orthogonal conformations can be detected, the dihedral angle (α_1) is scanned (see Fig. 6(a) and (b)). It is found that the oscillator strength could be enhanced to 0.0078 for PTZ-Ph-TTR and 0.0031 for PTZ-TTR. However, there is little energy variation for the dihedral angle changes from 90 degrees to 80 degrees. This means that it is quite easy for donors or acceptors to rotate at room temperature, and the rotation is also helpful for the emission of near-orthogonal conformations. Of course, we cannot exclude the influence of functionals adopted, since the oscillator strength is also quite dependent on the functionals especially for the CT states.⁴⁶

Table 4 Spin-orbit coupling (SOC) between S_1 and T_1 and radiative rates (k_r) from S_1 to S_0 . The intersystem crossing rates (k_{ISC}) and reverse intersystem crossing rates (k_{RISC}) between S_1 and T_1 are also listed

		SOC ^a (cm ⁻¹)	k_{ISC} (s ⁻¹)	SOC ^b (cm ⁻¹)	k_{RISC} (s ⁻¹)	k_r (s ⁻¹)
Toluene	PTZ-TTR-p	0.389	2.20×10^7	0.702	—	5.01×10^7
	PTZ-TTR-o	0.021	2.78×10^6	0.031	6.74×10^6	1.61×10^4
	PTZ-Ph-TTR-p	0.499	9.28×10^5	0.635	—	1.02×10^8
	PTZ-Ph-TTR-o	0.003	3.04×10^4	0.005	1.11×10^5	0
Aggregation	PTZ-TTR-p	0.409	4.60×10^7	0.993	—	2.58×10^7

^a SOC between S_1 and T_1 calculated based on the geometry of S_1 . ^b SOC between S_1 and T_1 calculated based on the geometry of T_1 .

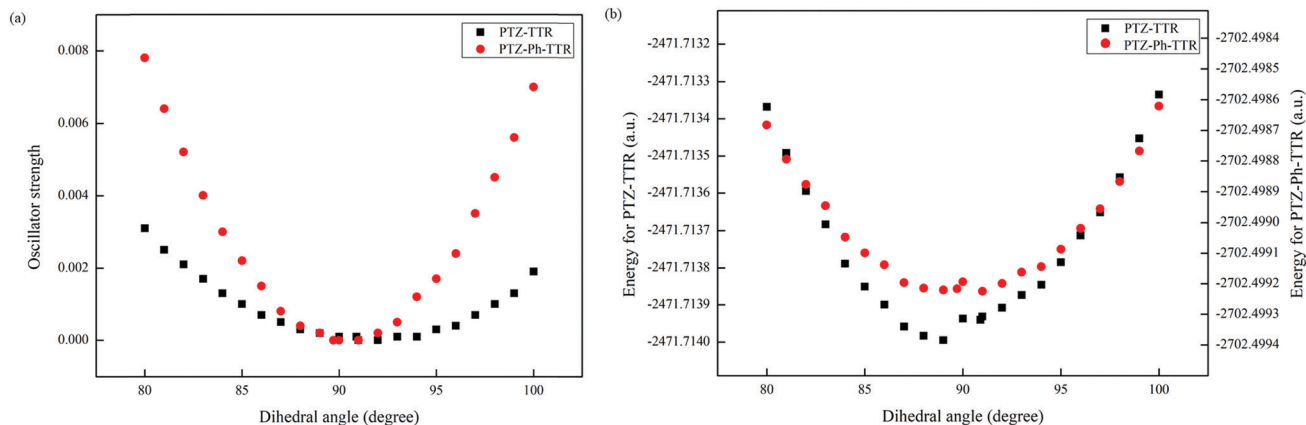


Fig. 6 Oscillator strength (a) and energy (b) of S_1 for PTZ-TTR and PTZ-Ph-TTR with different dihedral angles (α_1).

3.3 Aggregation effect

Since TADF molecules used in OLEDs are always in the aggregation state, the light-emitting properties should be different from those in toluene. The environmental effects on the light-emitting properties of the PTZ-TTR molecule are studied here. The models for PTZ-TTR in the aggregation state are simulated based on the crystal structures obtained experimentally (as shown in Fig. 1(b)).¹⁴ From the crystal structure, we find that there is only one conformation for PTZ-TTR. The near-orthogonal conformation does not exist, which is in agreement with our calculation results in toluene that PTZ-TTR-o is higher in energy than PTZ-TTR-p. In addition, it is quite easy for PTZ-TTR-o to transform into PTZ-TTR-p. Thus the photophysical properties of the PTZ-TTR-p molecule in the aggregation state are compared with those of PTZ-TTR-p in toluene. From the energy levels of excited states, we can see that there is also only one triplet state which is lower in energy than S_1 . However, the energy gap (0.48 eV) between them is much smaller than that in toluene (see Fig. S1, ESI[†]). Then both the S_1 and T_1 states are optimized in the aggregate state. It is found that the change of α_1 in aggregation is slightly larger than that in toluene by comparing the difference between S_0 and S_1 or S_1 and T_1 , while the variation of α_2 in the aggregate state (4° and 1°) is much smaller than that in toluene (16° and 6°). The RMSD values between S_1 and S_0 as well as between S_1 and T_1 are both smaller than those in toluene (Fig. S2, ESI[†]). This indicates that aggregation can effectively hinder the geometric change when the molecule transits in two states. Then the transition properties are analyzed as shown in Fig. S3 (ESI[†]). It is found that aggregation has only a little influence on the transition properties where the LE component is increased slightly. Besides, the SOC value between S_1 and T_1 and the ISC rates for PTZ-TTR in aggregation are also slightly enhanced compared to those in toluene (see Table 4). In addition, the radiative rate in the aggregation state is in the same order of magnitude as that in toluene.

3.4 Design of TADF molecules

Since PTZ-TTR is a typical D–A molecule that could realize dual emission and be applied in WOLEDs, we are wondering

whether other D–A molecules could also realize dual emission and be applied in WOLEDs. Consequently, several D–A molecules with different donors and the same acceptor unit are designed and studied (as shown in Fig. S4, ESI[†]). It can be found that the units PXZ, DMAC, DMAC-*t*Bu, DMDB, Cz, Cz-Me, and Cz-*t*Bu are adopted. First, the electron-donating ability is analyzed for all the systems based on the calculation of the charge difference of donors S_1 and S_0 (see Fig. S5, ESI[†]). It is obvious that the electron-donating ability of the donors is much higher in the near-orthogonal conformations than in the near-planar conformations. This should be due to more significant charge transfer in the near-orthogonal conformations when they transit between two states. For each type of conformation, the electron-donating ability of the donors changes a little except for the systems with DMDB. The significant deviation between the systems with DMDB and other donors should come from the difference in geometries. The most important parameter that determines the charge transfer properties is the dihedral angles between the donors and acceptors. Consequently, the dihedral angles (α_1) between D and A for all the systems are illustrated in Fig. 7(a). It can be found that α_1 for each near-orthogonal conformation is nearly 90 degrees, while the angle for each near-planar conformation is nearly zero. The angles for the “near-orthogonal” systems with DMDB are 38 degrees and 55 degrees, which is quite different from the other systems. Besides, the angles (α_4) are also studied. It can be found that the angle tends to be 180 degrees for all the near-orthogonal conformations, which means that the donor groups tend to be a plane in the near-orthogonal conformations. When the molecules exist in the near-planar conformation, the donor groups would bend at an angle of about 135 degrees. One should note that there is only one conformation for the systems with Cz groups, which should be due to the infeasibility for Cz bending. This indicates that only the systems with the six-membered heterocyclic compound in the donors could have dual conformations. Besides, the emission wavelengths of all the systems are also illustrated in Fig. 7(b). It can be found that the donors have a more obvious influence on the emission wavelengths of the

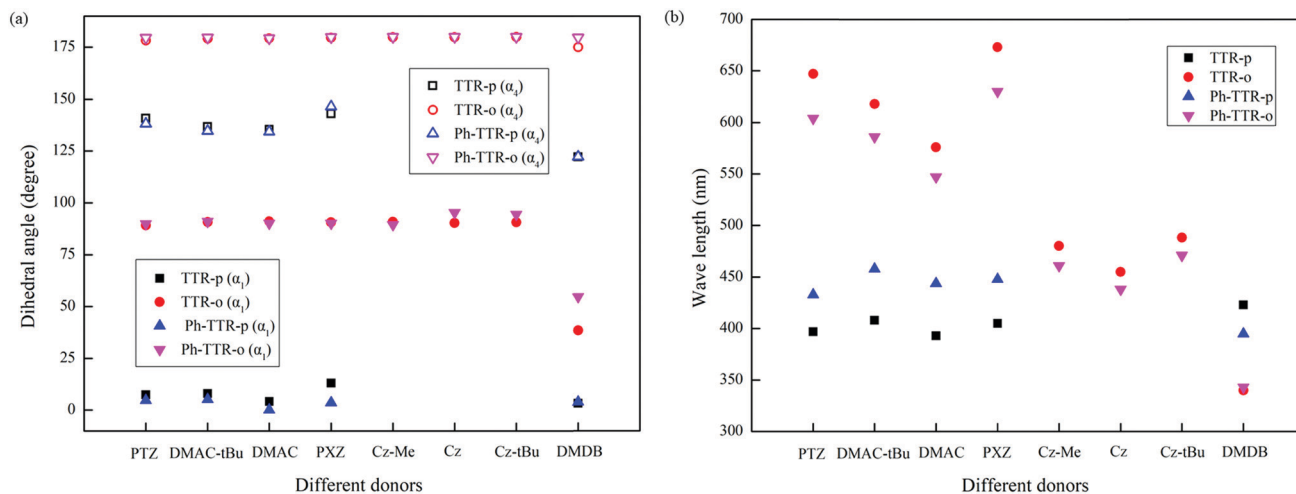


Fig. 7 Dihedral angles (α_1 and α_4) (a) and emission wavelengths (b) for all the systems.

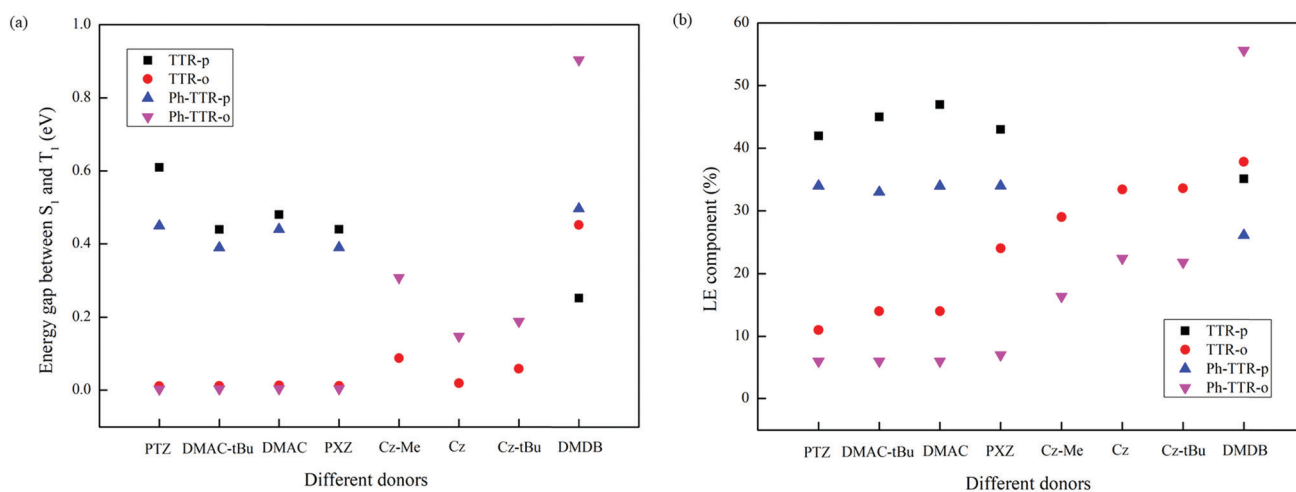


Fig. 8 S_1 - T_1 energy gaps (a) and LE components in the excitation of S_1 (b) for all the systems.

near-orthogonal conformations. It can also be seen that the emission wavelengths of the near-orthogonal conformations redshift with increasing electron-donating ability except for the systems with PXZ. This indicates that one should adopt the donors with a strong electron-donating ability to generate compensatory emissions if they want to use the systems as single emitters in WOLEDs. Specifically, our calculation results about the emission wavelengths indicate that DMAC-*t*Bu-TTR and PXZ-Ph-TTR based molecules are good candidates as single emitters in WOLEDs.

The S_1 - T_1 energy gaps for all the systems are also illustrated in Fig. 8(a). It can be seen that the energy gap for the near-orthogonal conformations is close to zero, while the gap for the near-planar conformations is 0.39 eV and even larger. In addition, we can also find that the energy gap for the Cz-based systems is larger than other systems except for the systems with DMDB. This indicates that both the Cz-based systems and the systems with DMDB are not good TADF candidates. Finally, we also investigated the LE components (see Fig. 8(b)) of NTOs (see Fig. S6-S8, ESI†)

in the excitation of S_1 . It is obvious that the LE components for all the near-orthogonal conformations significantly decrease with the enhancement of the electron-donating ability. However, the LE components for the near-planar conformations are only slightly influenced by the donors.

4. Conclusions

In summary, we systematically studied the light-emitting mechanism of PTZ-TTR and PTZ-Ph-TTR in toluene. For both molecules, dual complementary emission from two conformations is found. However, only one conformation (near-planar) is stable for PTZ-TTR in the ground state, which results in relatively weak orange emission from the near-orthogonal conformation that can only be generated by transformation from the near-planar conformation in excited states. For PTZ-Ph-TTR, both conformations are stable in the ground state, and thus the orange emission from the near-orthogonal

conformation which could be generated by direct excitation or by the transformation from the near-planar conformation in excited states is relatively stronger. Our calculation indicates that TADF could be realized due to the up-conversion from T_1 to S_1 in the near-orthogonal conformations. Besides, the up-conversion may also happen during the conformation transformation process since the crossing point is found for the S_1 and T_1 potential energy curves. By comparing the emission properties for PTZ-TTR in toluene and the aggregation state, we find that aggregation could induce a smaller energy gap between S_1 and T_1 . The substitution effect of donors on light-emitting properties is also studied, and the donors with six-membered heterocyclic compounds tend to form two conformations with dual emission. Donors with strong electron-donating ability are favorable for realizing compensatory emissions needed in WOLEDs. Our calculation results also propose that DMAC-*t*Bu-TTR and PXZ-Ph-TTR are potential emitters with dual emission used in WOLEDs.

Conflicts of interest

There are no competing financial interest.

Acknowledgements

This work was supported by the National Natural Science Foundation of China (Grant No. 11974216 and 11874242) and the Shandong Provincial Natural Science Foundation, China (ZR2019MA056). The authors thank the support from the Taishan Scholar Project of Shandong Province and the Project funded by China Postdoctoral Science Foundation (Grant No. 2018M642689).

References

- 1 C. W. Tang and S. A. VanSlyke, *Appl. Phys. Lett.*, 1987, **51**, 913.
- 2 S. Reineke, F. Lindner, G. Schwartz, N. Seidler, K. Walzer, B. Lüssem and K. Leo, *Nature*, 2009, **459**, 234.
- 3 J.-H. Jou, S. Kumar, A. Agrawal, T.-H. Li and S. Sahoo, *J. Mater. Chem. C*, 2015, **3**, 2974.
- 4 J. Ye, C. J. Zheng, X. M. Ou, X. H. Zhang, M. K. Fung and C. S. Lee, *Adv. Mater.*, 2012, **24**, 3410.
- 5 W. Liu, C.-J. Zheng, K. Wang, M. Zhang, D.-Y. Chen, S.-L. Tao, F. Li, Y.-P. Dong, C.-S. Lee and X.-M. Ou, *ACS Appl. Mater. Interfaces*, 2016, **8**, 32984.
- 6 X. L. Li, G. Xie, M. Liu, D. Chen, X. Cai, J. Peng, Y. Cao and S. J. Su, *Adv. Mater.*, 2016, **28**, 4614.
- 7 C. J. Zheng, J. Wang, J. Ye, M. F. Lo, X. K. Liu, M. K. Fung, X. H. Zhang and C. S. Lee, *Adv. Mater.*, 2013, **25**, 2205.
- 8 J. Kido, K. Hongawa, K. Okuyama and K. Nagai, *Appl. Phys. Lett.*, 1994, **64**, 815.
- 9 Y. Sun, N. C. Giebink, H. Kanno, B. Ma, M. E. Thompson and S. R. Forrest, *Nature*, 2006, **440**, 908.
- 10 L. Murphy, P. Brulatti, V. Fattori, M. Cocchi and J. G. Williams, *Chem. Commun.*, 2012, **48**, 5817.
- 11 W. X. Ni, M. Li, J. Zheng, S. Z. Zhan, Y. M. Qiu, S. W. Ng and D. Li, *Angew. Chem., Int. Ed.*, 2013, **52**, 13472.
- 12 H. Liu, X. Cheng, H. Zhang, Y. Wang, H. Zhang and S. Yamaguchi, *Chem. Commun.*, 2017, **53**, 7832.
- 13 I. E. Serdiuk, *J. Phys. Chem. C*, 2018, **122**, 18615.
- 14 K. Wang, Y.-Z. Shi, C.-J. Zheng, W. Liu, K. Liang, X. Li, M. Zhang, H. Lin, S.-L. Tao and C.-S. Lee, *ACS Appl. Mater. Interfaces*, 2018, **10**, 31515.
- 15 H. Wang, Y. Li, Y. Zhang, J. Mei and J. Su, *Chem. Commun.*, 2019, **55**, 1879.
- 16 M. Pan, W.-M. Liao, S.-Y. Yin, S.-S. Sun and C.-Y. Su, *Chem. Rev.*, 2018, **118**, 8889.
- 17 T. Tsuboi, *J. Non-Cryst. Solids*, 2010, **356**, 1919.
- 18 C. Zhou, S. Zhang, Y. Gao, H. Liu, T. Shan, X. Liang, B. Yang and Y. Ma, *Adv. Funct. Mater.*, 2018, **28**, 1802407.
- 19 Q. Zhang, B. Li, S. Huang, H. Nomura, H. Tanaka and C. Adachi, *Nat. Photonics*, 2014, **8**, 326.
- 20 X. Lv, R. Huang, S. Sun, Q. Zhang, S. Xiang, S. Ye, P. Leng, F. B. Dias and L. Wang, *ACS Appl. Mater. Interfaces*, 2019, **11**, 10758.
- 21 S. Hirata, Y. Sakai, K. Masui, H. Tanaka, S. Y. Lee, H. Nomura, N. Nakamura, M. Yasumatsu, H. Nakanotani and Q. Zhang, *Nat. Mater.*, 2015, **14**, 330.
- 22 L. Lin, J. Fan, L. Cai and C.-K. Wang, *Mol. Phys.*, 2018, **116**, 19.
- 23 L. Lin, L. Cai, J. Fan and C.-K. Wang, *J. Phys. Chem. C*, 2018, **122**, 19953.
- 24 J. Tomasi, B. Mennucci and R. Cammi, *Chem. Rev.*, 2005, **105**, 2999.
- 25 L. Lin, J. Fan, L. Cai and C.-K. Wang, *RSC Adv.*, 2017, **7**, 44089.
- 26 X. Zheng, Q. Peng, L. Zhu, Y. Xie, X. Huang and Z. Shuai, *Nanoscale*, 2016, **8**, 15173.
- 27 L. W. Chung, W. Sameera, R. Ramozzi, A. J. Page, M. Hatanaka, G. P. Petrova, T. V. Harris, X. Li, Z. Ke and F. Liu, *Chem. Rev.*, 2015, **115**, 5678.
- 28 J. Fan, Y. Zhang, Y. Zhou, L. Lin and C.-K. Wang, *J. Phys. Chem. C*, 2018, **122**, 2358.
- 29 K. Zhang, L. Cai, J. Fan, Y. Zhang, L. Lin and C.-K. Wang, *Spectrochim. Acta, Part A*, 2019, **209**, 248.
- 30 J. Fan, L. Cai, L. Lin and C.-K. Wang, *Phys. Chem. Chem. Phys.*, 2017, **19**, 29872.
- 31 J. Fan, L. Cai, L. Lin and C.-K. Wang, *J. Phys. Chem. A*, 2016, **120**, 9422.
- 32 M. Frisch, G. Trucks, H. Schlegel, G. Scuseria, M. Robb, J. Cheeseman, G. Scalmani, V. Barone, G. Petersson and H. Nakatsuji, *Gaussian 16, revision A.03*, Gaussian Inc., Wallingford, CT, 2016.
- 33 D. McCumber, *Phys. Rev.*, 1964, **136**, A954.
- 34 Z. Shuai, Q. Peng, Y. Niu and H. Geng, *MOMAP, a free and open-source molecular materials property prediction package*, Revision 0.2 4, 2014.
- 35 Z. Shuai, D. Wang, Q. Peng and H. Geng, *Acc. Chem. Res.*, 2014, **47**, 3301.
- 36 Q. Peng, Y. Niu, Q. Shi, X. Gao and Z. Shuai, *J. Chem. Theory Comput.*, 2013, **9**, 1132.

- 37 Y. Niu, Q. Peng, C. Deng, X. Gao and Z. Shuai, *J. Phys. Chem. A*, 2010, **114**, 7817.
- 38 T. Lu and F. Chen, *J. Comput. Chem.*, 2012, **33**, 580.
- 39 Y. Cao, J. Eng and T. Penfold, *J. Phys. Chem. A*, 2019, **123**, 2640.
- 40 R. L. Martin, *J. Chem. Phys.*, 2003, **118**, 4775.
- 41 A.-D. Gorse and M. Pesquer, *J. Phys. Chem.*, 1995, **99**, 4039.
- 42 R. Chen, Y. Tang, Y. Wan, T. Chen, C. Zheng, Y. Qi, Y. Cheng and W. Huang, *Sci. Rep.*, 2017, **7**, 6225.
- 43 Y. Pan, W. Li, S. Zhang, L. Yao, C. Gu, H. Xu, B. Yang and Y. Ma, *Adv. Opt. Mater.*, 2014, **2**, 510.
- 44 C. Angeli, K. Bak, V. Bakken, O. Christiansen, R. Cimiraglia, S. Coriani, P. Dahle, E. Dalskov, T. Enevoldsen and B. Fernandez, see <http://www.daltonprogram.org>.
- 45 J. Gibson, A. P. Monkman and T. J. Penfold, *ChemPhysChem*, 2016, **17**, 2956.
- 46 M. Caricato, G. W. Trucks, M. J. Frisch and K. B. Wiberg, *J. Chem. Theory Comput.*, 2010, **7**, 456.